Available online at www.sciencedirect.com
SCIENCE DIRECT®
Journal of Solid State Chemistry 178 (2005) 3381–3388
JOURNAL OF SOLID STATE CHEMISTRY
www.elsevier.com/locate/jssc

Hydrides with the perovskite structure: General bonding and stability considerations and the new representative $CaNiH_3$

Toyoto Sato[a], Dag Noréus[a], Hiroyuki Takeshita[b], Ulrich Häussermann[c,*]

[a]*Structural Chemistry, Stockholm University, 10691 Stockholm, Sweden*
[b]*Department of Materials Science and Engineering, Faculty of Engineering, Kansai University, Yamate-cho, Suita, Osaka 564-8680, Japan*
[c]*Inorganic Chemistry, Stockholm University, 10691 Stockholm, Sweden*

Received 27 May 2005; received in revised form 16 August 2005; accepted 28 August 2005
Available online 3 October 2005

Abstract

The stability and electronic structure of perovskite hydrides ABH_3 were investigated by means of first-principles density functional calculations. Two types of perovskite hydrides are distinguished: (1) When A and B are alkali and alkaline earth metals, the hydrides are ionic compounds with calculated band gaps of around 2 eV and higher. Their stability trend follows basically the concept of Goldschmidt's tolerance factor. (2) When A is one of the heavier alkaline earth metals (Ca, Sr, Ba) and B a transition metal, stable compounds ABH_3 result only when B is from the Fe, Co, or Ni groups. This stability trend is basically determined by effects associated with d band filling of both the transition metal and the hydride. In contrast to group (1) perovskites, the transition metal-containing compounds are metals. The synthesis of $CaNiH_3$ and its structure determination from $CaNiD_3$ is reported. This compound is a type (2) perovskite hydride with a fully occupied hydrogen position ($CaNiD_3$: $a = 3.551(4)$ Å, $d_{Ni-D} = 1.776(2)$ Å). Its stability is discussed with respect to transition metal hydrides with complex anions (e.g., Mg_2NiH_4, Na_2PdH_2, Sr_2PdH_4).

Keywords: Perovskite structure; Metal hydrides; First-principles calculations

1. Introduction

Perovskites ABX_3 represent an enormously prolific family of inorganic compounds. They constitute of two differently sized metal cations A and B and anions X from the chalcogen or halogen groups. Ideal perovskites adopt the cubic space group $Pm\bar{3}m$, where X anions centre the cell edges at $3d$ (1/2,0,0) and A- and B-type cations are located at the cell centre and corners, respectively (Fig. 1). Thus, B-type cations are octahedrally and A-type cations are cuboctahedrally coordinated by X. Usually, $SrTiO_3$ is considered as the archetype of the ideal perovskite structure. However, most perovskites appear distorted and crystallise in a lower symmetric space group. This gives rise to diverse magnetic and electric properties, which make perovskites interesting and important for technological applications [1].

Besides chalcogenides and halogenides, there are a few examples of perovskite hydrides ($X = H$). In the case of A and B being a monovalent alkali metal (M) and a divalent alkaline earth metal (Ae), the ternary metal hydrides have a saline bonding character. Such hydrides are of interest for hydrogen storage at high temperature. There are five reported hydrides with the ideal $Pm\bar{3}m$ perovskite structure: $CsCaH_3$, $RbCaH_3$, $KMgH_3$, $BaLiH_3$, and $SrLiH_3$ [2–5]. The latter are sometimes referred to as inverse perovskites since the singly charged M cation occupies the octahedral voids. Additionally, it has been proposed that the light metal hydride $LiBeH_3$ adopts the cubic perovskite structure and displays high-temperature superconductivity [6]. However, the structure and properties of $LiBeH_3$ have been questioned [7].

Interestingly, there is a second group of perovskite hydrides, consisting of a divalent metal and the transition metal Pd. These hydrides—$CaPdH_2$, $SrPdH_{2.7}$, $YbNiH_{2.7}$, $YbPdH_{2.7}$, and $EuPdH_{2.9}$ [8–11]—exhibit a variable degree of hydrogen deficiency with respect to the ideal perovskite composition. In this work we attempt to rationalise bonding

*Corresponding author.
E-mail addresses: dag@struc.su.se (D. Noréus), ulrich@inorg.su.se (U. Häussermann).

0022-4596/$ - see front matter © 2005 Elsevier Inc. All rights reserved.
doi:10.1016/j.jssc.2005.08.026

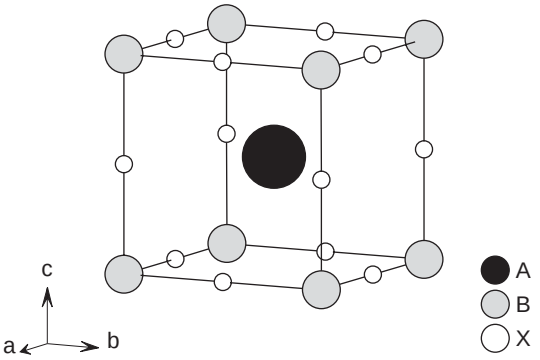

Fig. 1. Cubic perovskite structure.

and stability of perovskite hydrides. The bonding properties of the transition metal-containing compounds should be rather different from that of the saline compounds. Additionally, we report on the synthesis and structural characterisation of $CaNiH_3$, which represents a stoichiometric transition metal, perovskite hydride. This is in contrast to $CaPdH_2$, which allegedly consists of statistically disordered linear complexes $[PdH_2]^{2-}$ [8]. Such molecular units had previously been identified in Li_2PdH_2 and Na_2PdH_2 [12,13]. In this respect reports from Orimo et al. [14] and Chen et al. [15] on amorphous $MgNiH_{1.9}$ and $MgNiH_{2.2}$, respectively, are interesting. The radial distribution function of $MgNiH_{1.9}$ obtained from the measured neutron diffraction pattern was interpreted with a coordination of two for deuterium around nickel with an Ni–D distance of 1.7(3) Å [16]. This could indicate a possible linear NiH_2 unit, similar to what has previously been found with palladium.

No 1:1 Ca:Ni intermetallic compound exists and the 1:1 ratio in the $CaNiH_3$ hydride is maintained with the support of hydride ions. The instability of the metal atom framework without the support of hydrogen also seems to have some consequences for the synthesis of $CaNiH_3$. This hydride could not be obtained by sintering CaH_2 and nickel powder in hydrogen up to 5 MPa using various sintering temperatures up to 623 K. Takeshita et al. [17] found what was assumed to be $CaNiH_3$ by carefully disproportioning a $CaNi_3$ hydride. Kakuta et al. [18] reported similar results when they reacted a CaH_2–33 at% Ni mixture in an anvil cell at 5 GPa and 1073 K. But in this case, the deuteride prerequisite for full structural refinement was not synthesised. In the present work, we prepared $CaNiH_3$ and $CaNiD_3$ by reacting mixtures of $CaNi_3$ and Ca_2Ni_7 alloys with hydrogen or deuterium in a rather elaborate scheme and the structure was obtained from neutron diffraction data of the deuteride.

2. Experimental

2.1. Synthesis and characterisation of $CaNiH_3$

Commercially pure granular Ca and Ni powders were used as starting materials. The Ca granules were cut into finer grains and mixed with Ni powder in a molar ratio Ca:Ni = 1:2. The metal mixture was pressed into pellets and the pellets were put into an aluminium oxide tube, which was reacted in a stainless steel reactor. The reactor was heated at 10 K/min from 293 to 898 K, then kept at 898 K for 125 min, heated again at 10 K/min to 1073 K, kept at this temperature for 120 min and finally cooled to room temperature. The obtained product was crushed, further Ni powder was added, and the mixtures were again pressed into pellets. The pellets were reacted using a similar procedure as above, but with the final temperature set to 1123 K. The final product was a mixture of $CaNi_3$ and Ca_2Ni_7 with some CaO impurity. The mixture of Ca–Ni alloys was deuterated at 473 K at a pressure of 40 kg/cm^2 for 7 days in a stainless steel reaction tube. In order to optimise the reacting conditions, initial tries were made using hydrogen where reaction time, pressure and temperature were varied.

Hydrided and deuterated Ca–Ni alloys were investigated by X-ray powder diffraction with a Guinier–Hägg focusing camera of 40 mm diameter, using monochromatised Cu$K\alpha_1$ radiation ($\lambda = 1.5405980$ Å). Si ($a = 5.430879$ Å at 298 K) was added as an internal standard. The films obtained were measured in an LS 18 film scanner [19]. The program SCANPI [20] was used to evaluate the photographs, and the programs TREOR [21] and PIRUM [22] were used to index the patterns. The deuterated sample was measured by powder neutron diffraction ($\lambda = 1.47$ Å) from $2\theta = 4.00^\circ - 139.92^\circ$ in steps of $\Delta(2\theta) = 0.08^\circ$ at 295 K, at NFL, Studsvik, Sweden. The Rietveld program Fullprof was used for profile refinement of the powder neutron diffraction data [23].

2.2. Electronic structure calculations

Total energy calculations for perovskite hydrides ABH_3 were performed in the framework of the frozen core all-electron Projected Augmented Wave method [24], as implemented in the program VASP [25]. The energy cut-off was set to 500 eV. Exchange and correlation effects were treated by the generalised gradient approximation, usually referred to as PW91 [26]. The integration over the Brillouin zone was done on special k-points determined according to the Monkhorst–Pack scheme [27]. All necessary convergence tests were performed and total energies were converged to at least 1 meV/atom. The equilibrium volume V_{eq} and the corresponding energy E_{eq} were obtained by fitting E vs. V values to a Birch–Murnaghan equation of state. The theoretical equilibrium lattice parameter and some physical properties of the experimentally known compounds are collected in Table 1. With the exception of $SrLiH_3$, the deviation between experimental and theoretical lattice parameter is 0.5% or lower. In order to assess zero Kelvin energies of formation for ABH_3, the same procedure was applied for hydrides AeH_2 (Ae = alkaline earth metal) and MH (M = alkali metal). MH was considered in the cubic NaCl structure, and AeH_2 in the

Table 1
Calculated lattice parameters (a), bulk moduli (B_0) and band gaps (e_g) of the investigated hydrides

	a (Å)	B_0 (GPa)	e_g (eV)
$CsCaH_3$	4.6169 (4.609)	23.5	3.17
$RbCaH_3$	4.5326 (4.547)	24.3	3.32
$KMgH_3$	4.0181 (4.018)	34.5	2.59
$BaLiH_3$	4.0148 (4.023)	38.2	2.28
$SrLiH_3$	3.8044 (3.833)	42.8	1.93
$CaNiH_3$	3.5262 (3.544)	93.2	—
$SrPdH_3$	3.8490 (3.843)	82.3	—
$CaPdH_3$	3.7273	90.8	—
$CaPdH_2$	3.6997 (3.69)	79.9	—

Experimental values for a are given in parentheses.

tetragonal rutile (Ae = Be, Mg) and orthorhombic $BaCl_2$-type structure (Ae = Ca, Sr, Ba).

3. Results and discussion

3.1. Saline perovskites $MAeH_3$ and (anti-perovskites) $AeMH_3$

We calculated energies for the formation reactions

$$MH + AeH_2 \rightarrow MAeH_3$$
(M = Li, Na, K, Rb, Cs; Ae = Be, Mg, Ca)

and

$$AeH_2 + MH \rightarrow AeMH_3$$
(Ae = Be, Mg, Ca, Sr, Ba; M = Li, Na, K).

The results are depicted in Figs. 2a and b. Concerning perovskites $MAeH_3$, we obtain negative formation energies for $MMgH_3$ with M = Na, K, Rb, Cs. This agrees well with the experimental observations. The formation energy for $NaMgH_3$ in the $Pm\bar{3}m$ perovskite structure is only slightly negative. Indeed, $NaMgH_3$ crystallises in an orthorhombically distorted perovskite structure (i.e., the $GdFeO_3$ type) [28]. We calculated that the stabilisation over the ideal perovskite structure is about 0.09 eV/Z. $KMgH_3$ has the most negative formation energy in the series of Mg compounds and crystallises with the ideal perovskite structure [4]. The ideal perovskite formation energy of $RbMgH_3$ is somewhat higher than that of $KMgH_3$. This compound adopts the hexagonal $BaTiO_3$ structure, which is a 6H stacking variant of the hexagonal perovskite structure [29]. As for $NaMgH_3$, the formation energy for $CsMgH_3$ is only slightly negative. This indicates that a compound with this composition should be stable, but unlikely to crystallise in the ideal perovskite structure. Experimentally, it has been found that $CsMgH_3$ has a low- and a high-pressure form [30]. The structures of both modifications are not related to the ideal perovskite structure. Also, $CsCaH_3$ and $RbCaH_3$ are reported to adopt the ideal cubic $Pm\bar{3}m$ perovskite structure [2,3]. For

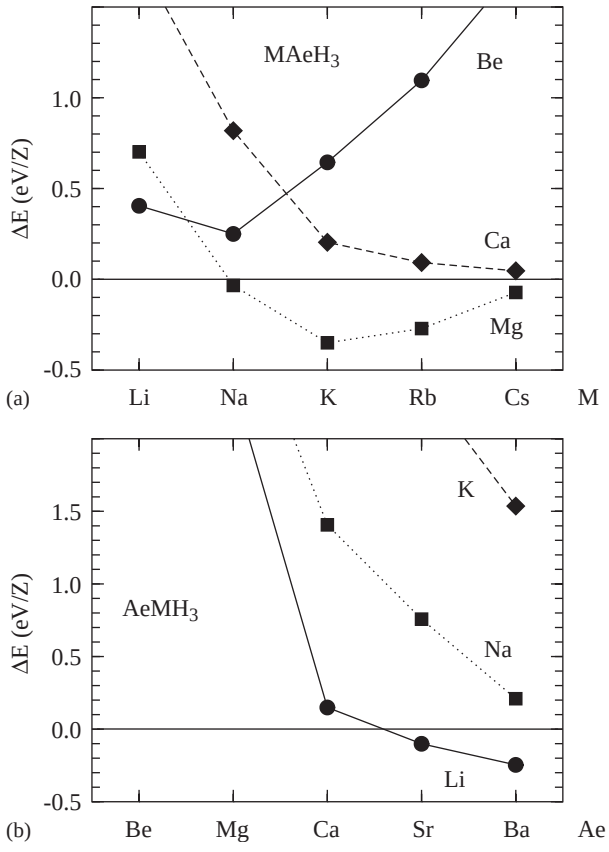

Fig. 2. Energies of formation with respect to AeH_2 and MH for $MAeH_3$ (Ae = Be, Mg, Ca) (a) and $AeMH_3$ (M = Li, Na, K) (b).

these compounds, however, our calculations yield slightly positive formation energies [31]. Turning to anti-perovskites $AeMH_3$, only $BaLiH_3$ and $SrLiH_3$ yield negative energies of formation. Indeed, these two compounds adopt this structure type [5].

The stability of the ideal cubic perovskite structure is usually discussed using the Goldschmidt tolerance factor $t = (r_X + r_A)/[\sqrt{2}(r_X + r_B)]$. This factor becomes unity if $r_X = r_A$, i.e., X and A form an ideal cubic close packing of spheres and B fits the octahedral voids perfectly ($r_B = (\sqrt{2} - 1)r_A(r_X)$) [1]. For the calculation of t ionic radii are employed, i.e., purely ionic bonding is assumed. Empirically, it has been observed that the $Pm\bar{3}m$ structure occurs for t between 0.9 and 1 (for the archetype $SrTiO_3$ t = 1.002). Fig. 3 compiles t for $MAeH_3$ and $AeMH_3$ assuming a radius of 1.3 Å for H^- and using the Shannon radii for 12-coordinated M^+ and six-coordinated Ae^{2+} and vice versa for the anti-perovskites. As can be seen, the t values for the systems realising the $Pm\bar{3}m$ structure fall in the range between 0.92 and 1.01, which is in agreement with the general observation. For each series $MAeH_3$ (Ae = Be, Mg, Ca) and $AeMH_3$ (M = Li, Na, K), the system with a t value closest to unity also corresponds to the most stable with respect to the decomposition into binary hydrides. This justifies the ionic bonding description of this class of perovskite hydrides.

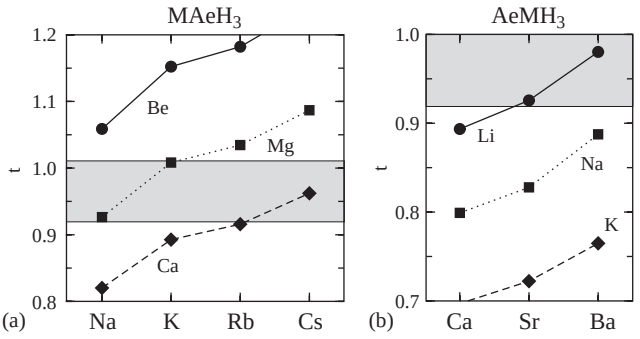

Fig. 3. Goldschmidt tolerance factors t for $MAeH_3$ (Ae = Be, Mg, Ca) (a) and $AeMH_3$ (M = Li, Na, K). Stable perovskites are found in the grey areas.

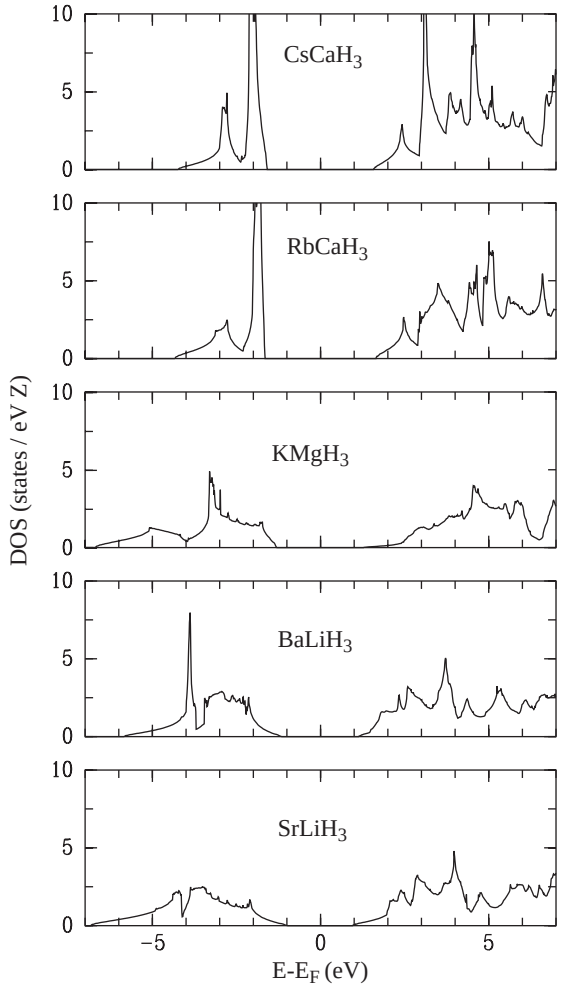

Fig. 4. Density of states for the ideal perovskites $CsCaH_3$, $RbCaH_3$, $KMgH_3$, $BaLiH_3$ and $SrLiH_3$ at their theoretical equilibrium volume.

As expected, the electronic structure of the saline perovskite hydrides is very similar. Fig. 4 shows the electronic density of states (DOS) of the stable perovskite hydrides. Additionally, in Fig. 5 the band structure of $CsCaH_3$ is depicted. We denote the three occupied bands arising from the hydrogen states as a_{1g} and e_g according to

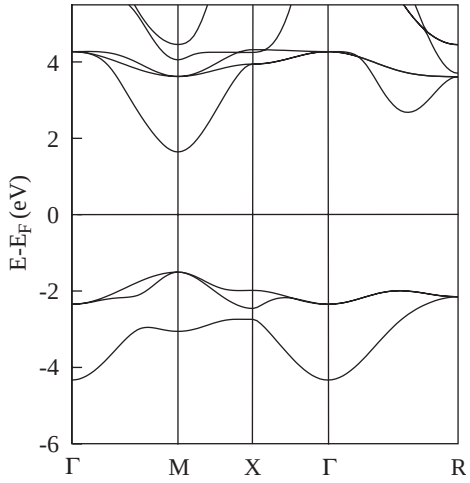

Fig. 5. Band structure of $CsCaH_3$.

their transformation behaviour at Γ. This splitting at Γ gives rise to a characteristic two-peak shape in the DOS of $CsCaH_3$ below the Fermi level. The lower lying a_{1g} band has a dispersion of about 2 eV, and the narrower e_g band of about 0.5 eV. $CsCaH_3$ is an insulator with a band gap of 3.17 eV. The calculated band gap in the saline perovskites reduces with decreasing lattice parameter. For $SrLiH_3$ with $a = 3.846$ Å (H–H distance 2.72 Å), the size of the band gap is 1.97 eV. At the same time, the dispersion of the occupied bands increases to about 6 eV and the two-peak shape of the occupied states disappears. Importantly, the increasing dispersion of the occupied bands with decreasing lattice parameter is accompanied by an increasing admixture of states from the small and polarising cations Mg or Li. This is essential for the stabilisation of this class of hydride compounds. Previously, Orgaz and Gupta analysed the electronic structure of $SrLiH_3$ and $BaLiH_3$ [32]. Their results are very similar to ours.

3.2. The new representative $CaNiH_3$

The X-ray diffraction pattern of hydrided Ca–Ni alloys could be indexed with a cubic unit cell $a = 3.544(1)$ Å, which is in agreement with $CaNiH_3$ as reported by Takeshita et al. [17] and Kakuta et al. [18]. The unit cell of deuterated $CaNiD_3$ was determined as $a = 3.5437(8)$ Å. The observed and calculated 2θ, d-values and X-ray intensities are shown in Table 2, indicating a CsCl-type structure for the metal atoms in $CaNiH_3$.

The refinement of the neutron diffraction pattern was made assuming the perovskite structure for $CaNiD_3$ as shown in Table 3. The Ni–D distance is 1.776(2) Å and the D–D distance 2.511(2) Å. Observed and calculated intensities from the Rietveld refinement are shown in Fig. 6. Three impurity phases were identified: Ni, $CaNi_5$ and CaO. All were included in the refinement. The refined weight fractions of the participating phases were $CaNiD_3$ 51(2)%, Ni 32(2)%, $CaNi_5$ 9(1)% and CaO 8(1)%. Ni is thus the

Table 2
Observed and calculated 2θ, d-values and X-ray intensities for $CaNiD_3$

$h\,k\,l$	$2\theta_{obs}$	$2\theta_{cal}$	d_{obs}	d_{cal}	I_{obs}	I_{cal}
1 0 0	25.043	25.059	3.5529	3.5507	2	1
1 1 0	35.788	35.733	2.5070	2.5108	100	100
1 1 1	44.421	44.142	2.0378	2.0500	<1	<1
2 0 0	51.471	51.471	1.7740	1.7753	16	14
2 1 1	64.059	64.200	1.4524	1.4496	28	23
2 2 0	75.627	75.701	1.2554	1.2551	7	6

$M(6) = 46$.

Table 3
Refinement results for $CaNiD_3$ (space group $Pm\bar{3}m$ (no. 221) and $Z = 1$)

Atom	Site	x	y	z	B_{iso}	Occupancy
Ni	1*a*	0	0	0	0.2(2)	1.0
Ca	1*b*	1/2	1/2	1/2	0.6(5)	1.0
D	3*d*	1/2	0	0	2.4(5)	1.0
	R_B (%)	R_F (%)	Wt. fraction (%)			
$CaNiD_3$	4.40	2.47	52(2)			
Ni	4.13	1.97	32(2)			
$CaNi_5$	19.3	13.6	9(1)			
CaO	11.5	14.0	8(1)			

$R_{wp} = 20.1\%$.

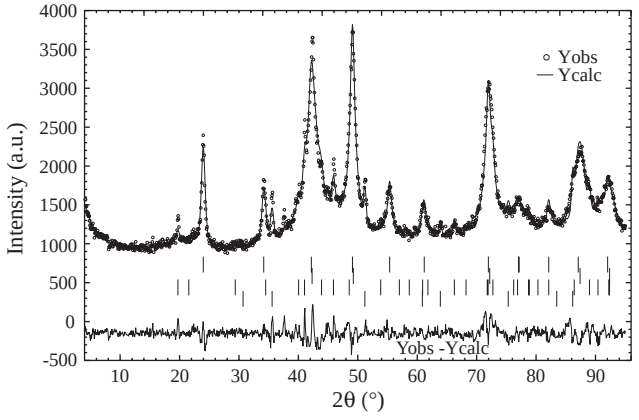

Fig. 6. Rietveld profile refinement of powder neutron diffraction data (o) for $CaNiD_3$ in space group $Pm\bar{3}m$ (no. 221). Reflection markers are for $CaNiD_3$, Ni, $CaNi_5$ and CaO (from above), respectively.

dominating impurity. Both the $CaNiD_3$ and Ni phases were of a poor crystal quality as reflected in the rather broad diffraction lines. This is understandable because during the hydrogenation reaction, which is performed at rather low temperatures, a major rearrangement of the metal atoms takes place, e.g., $CaNi_3 + 3/2H_2 = CaNiH_3 + Ni$. The decomposition reaction $CaNiH_3 = CaH_2 + Ni$ occurs at 748 K in an H_2 atmosphere [17], which prevents the employment of heat treatments for improving crystal quality. The unit cell dimension of $CaNi_5$ was refined to $a = 4.958$ and $c = 3.932$ Å in close agreement with a pure alloy not containing hydrogen. The very similar unit cell axis values for $CaNiD_3$ and Ni lead to problems with the overlapping peaks in the refinement. The Rietveld refined cell parameters were 3.538 and 3.528 Å, respectively. These values are, however, less accurate than the values obtained from the X-ray diffraction using an internal standard to correct the 2θ scale of the patterns. The peak width parameters could not be refined simultaneously, but were estimated from the diffraction pattern and kept fixed during the refinements. The major misfits in the diffraction pattern also occur where the diffraction peaks of $CaNiD_3$ and Ni overlap. Fortunately, both structures are very simple with no positional parameters to refine. Refining the occupancy of the deuterium atom position led to a slightly higher (within one standard deviation) occupancy than one. We thus assume that $CaNiD_3$ can be described with an ideal ABH_3 perovskite structure type having a hydrogen capacity corresponding to 2.95 wt%. This is also in agreement with the earlier performed volumetric determination of the hydrogen content [17], but is in contrast to $YbNiH_{2.7}$, $CaPdH_2$, $YbPdH_{2.7}$ and $EuPdH_{2.9}$ displaying the same kind of CsCl-type metal arrangement.

The band structure and DOS of $CaNiH_3$ are shown in Figs. 7 and 8, respectively. The small lattice parameter of 3.5262 Å implies a wide dispersion of the hydrogen-based bands. In $CaNiH_3$, the a_{1g}–e_g splitting of these bands is pronounced. The lower lying a_{1g} band is dispersed over a region from −10 to −6 eV below the Fermi level. This band contains a stabilising contribution from the Ni-*s* state. Compared to the a_{1g} band, the e_g band is rather narrow and confined between −6.5 and −5.5 eV. Due to a substantial admixture of Ni e_g *d* states, this band is essentially responsible for Ni–H bonding. At −2 eV the basically dispersionless, non-bonding, Ni t_{2g} *d* states are

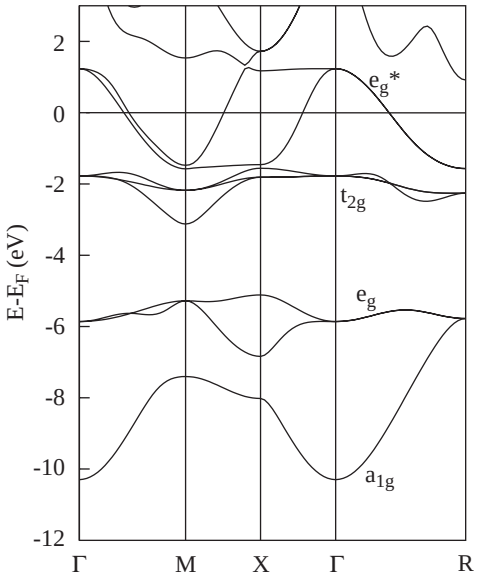

Fig. 7. Band structure of $CaNiH_3$ at the theoretical equilibrium volume.

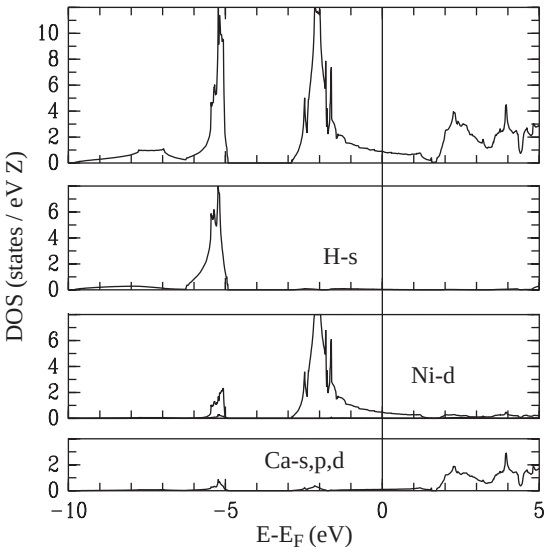

Fig. 8. Total density of states of $CaNiH_3$ and its decomposition into H-*s*, Ni-*d* and Ca-*s*,*p*,*d* contributions (from above).

centred. At even higher energies, from −1.5 to 1.5 eV, the Ni–H antibonding e_g band is distributed. This band is only half filled, which makes $CaNiH_3$ a metallic conductor. A completely filled e_g^* band would put the Fermi level at the pseudo-gap at 1.5 eV. The contribution of Ca states to the bands below the Fermi level is small. This suggests considering $CaNiH_3$ as consisting of a polyanionic framework $[NiH_3]^{2-}$ counterbalanced by Ca^{2+} cations. Thus, bonding in metallic $CaNiH_3$ appears rather different compared to the saline, insulating, perovskites. This is also indicated in the considerably higher bulk modulus (lower compressibility) of $CaNiH_3$ compared to that of the saline pervoskite hydrides.

3.3. Perovskites $AeTH_3$

Hitherto transition metal hydride perovskites $AeTH_3$ have been found with T = Ni, Pd and divalent Ae = Ca, Sr, Yb, Eu. The reported variable hydrogen deficiency of most of these compounds appears suspicious. Apart from $CaPdH_2$ their hydrogen content is close to the stoichiometric value of 3 (i.e., in a range of 2.7–2.9; as a matter of fact we cannot rule out such a slight hydrogen deficiency for $CaNiH_3$ either). The electronic structure of Pd perovskite hydrides has been previously investigated by Orgaz et al. [33] by employing the augmented plane wave method. In this work, hydrogen deficiency in $CaPdH_2$ was simulated by taking a weighed average of the structure factor over the three H sites, whereas for the other compounds a stoichiometric composition was assumed. The DOS for $SrPdH_3$ is similar to that of $CaNiH_3$ (cf. Fig. 8). The main difference is that the gap between the e_g and t_{2g} band is not present for $SrPdH_3$ due to the lower lying Pd-d states. The large degree of H deficiency of $CaPdH_2$ is remarkable. The computationally obtained

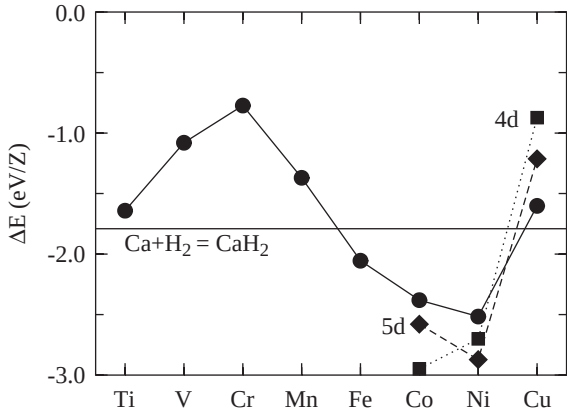

Fig. 9. Energy of formation with respect to the elements for $CaTH_3$ (T = Ti–Cu, Rh–Ag, Ir–Au).

equilibrium lattice parameter for $CaPdH_3$ is $a = 3.727$ Å (cf. Table 1). When applying the virtual crystal approximation for describing randomly H-deficient $CaPdH_2$, the lattice parameter reduces to 3.700 Å, which is close to the experimental value ($a = 3.69$ Å) [34]. On the other hand, the calculated equilibrium lattice parameter for $SrPdH_3$ and the experimental value for $SrPdH_{2.7}$ are in good agreement (cf. Table 1). Thus, our calculations corroborate hydrogen deficiency for the Ca compound. We return to this issue at the end of this chapter.

It is interesting to speculate on the general possibility to obtain transition metal-containing hydrogen perovskites $AeTH_3$. Fig. 9 gives a summary of the formation energies

$$Ca + T + 3/2H_2 \rightarrow CaTH_3$$
$$(T = Ti{-}Cu,\ Rh{-}Ag,\ Ir{-}Au).$$

In these calculations, all components were treated as nonmagnetic. The shape of the Ca-curve is a result of the different stability trends of T and $CaTH_3$ upon d band filling: The maximum for $CaCrH_3$ appears as a consequence of the high stability (large energy of cohesion) of elemental Cr with a half-filled d band. Perovskites $CaTH_3$ are most stable for T = Mn. This becomes clear from Fig. 10 where the DOS of $CaTH_3$ (T = Ti–Cu) at the computed equilibrium volumes are compiled. For T = Ti and V the nonbonding t_{2g} and antibonding e_g band are separated by a small gap which turns into a pseudo-gap for T = Cr and Mn. For T = Mn the Fermi level is exactly at this pseudo-gap, i.e., a situation is entered where the t_{2g} band is completely filled and the e_g band empty. Starting off T = Fe the t_{2g} and e_g bands merge and instead a separation of the e_g^* and the high-lying Ca-based bands appear. For $CaCuH_3$, the e_g^* band is completely filled. The minimum in the formation energy curve at T = Ni is a consequence of the more rapidly increasing destabilisation of T with increasing d band filling compared to $CaTH_3$. Taking into account the formation energy of CaH_2 (indicated in Fig. 9) perovskite hydrides are only stable for T = Fe, Co, Ni. The trend in the formation energy is

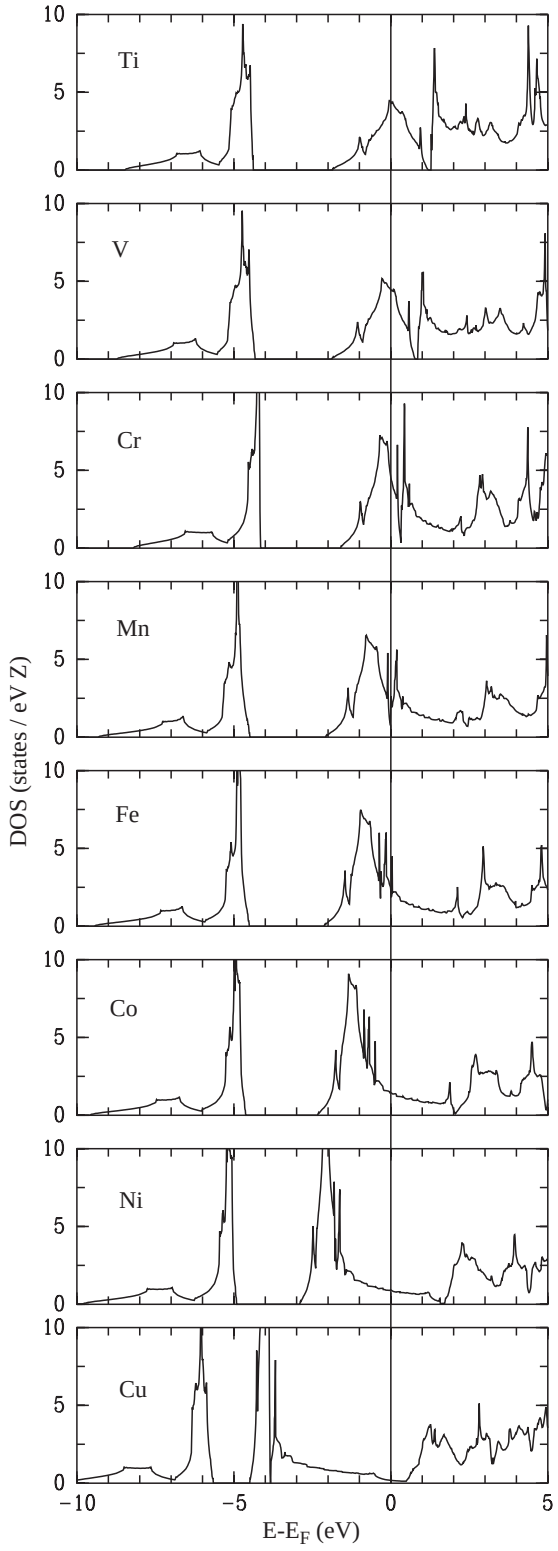

Fig. 10. Density of states for the ideal perovskites $CaTH_3$ (T = Ti–Cu) at their theoretical equilibrium volume.

similar for the T = 4d, 5d and/or Ae = Sr, Ba: Transition metal perovskite hydrides are most stable with respect to the decomposition into the elements when T is a group 9 or 10 metal. Interestingly, a similar stability and electronic structure trend was found for hypothetical $MgTH_3$ compounds as recently reported by Vegge et al. [35].

The stability of transition metal perovskite hydrides with polyanionic assemblies $[TH_3]^{2-}$ (T = Ni, Pd) has especially to be considered with respect to more hydrogen-rich transition metal hydride compounds containing isolated homoleptic complexes TH_n^{m-} with formally zero-valent T. Examples are Mg_2NiH_4 and Sr_2PdH_4 with tetrahedral $[TH_4]^{4-}$ [36,37], $NaBaH_3$ with trigonal planar $[TH_3]^{3-}$ [38] and Na_2PdH_2 with linear $[TH_2]^{2-}$ [13]. Nonstoichiometric perovskite hydrides—if existing—could actually consist of a mixture of polyanionic $[TH_3]^{2-}$ and linear $[TH_2]^{2-}$ entities. For $CaPdH_2$ it has been proposed that the perovskite structure may be a consequence of linear PdH_2^{2-} hydrido complexes randomly oriented along the cubic unit cell edges [8]. However, a careful reinvestigation of these systems has to be performed in order to corroborate this idea.

Acknowledgment

Financial support has been obtained from the HYSTORY project under the European Commission 5FP EESD program and by the Swedish Research Council (VR). Håkan Rundlöf, NFL, Studsvik, Sweden, is acknowledged for collecting the powder neutron diffraction data.

References

[1] R.H. Mitchell, Perovskites: Modern and Ancient, Almaz Press Inc., Thunder Bay, Ont., Canada, 2002.
[2] H.H. Park, M. Pezat, B. Darriet, Rev. Chim. Min. 23 (1986) 323.
[3] H.H. Park, M. Pezat, B. Darriet, C.R. Acad. Sc. 306 (1988) 963.
[4] R. Schuhmacher, A. Weiss, J. Less-Common Met. 163 (1990) 179.
[5] C.E. Messer, J.C. Eastman, R.G. Mers, A.J. Maeland, Inorg. Chem. 3 (1964) 776.
[6] A.W. Overhauser, Phys. Rev. B 35 (1987) 411.
[7] J.P. Bastide, Solid State Commun. 74 (1990) 355.
[8] W. Bronger, K. Jansen, P. Müller, J. Less-Common Met. 161 (1990) 299.
[9] W. Bronger, G. Ridder, J. Alloys Compd. 210 (1994) 53.
[10] K. Ensslen, E. Bucher, H. Oesterreicher, J. Less-Common Met. 92 (1983) 343.
[11] K.H.J. Buschow, R.L. Cohen, K.W. West, J. Appl. Phys. 48 (1977) 5289.
[12] K. Kadir, D. Noréus, Z. Phys. Chem. NF 163 (1989) 231.
[13] D. Noréus, K.W. Törnroos, A. Börje, T. Szabo, W. Bronger, H. Spittank, G. Auffermann, P. Müller, J. Less-Common Met. 139 (1988) 233.
[14] S. Orimo, K. Ikeda, H. Fujii, Y. Fujikawa, Y. Kitano, K. Yamamoto, Acta Mater. 45 (1997) 2271.
[15] J. Chen, T. Sakai, N. Kitamura, H.T. Takeshita, N. Kuriyama, J. Am. Chem. Soc. 123 (2001) 6193.
[16] S. Orimo, K. Ikeda, H. Fujii, S. Saruki, T. Fukunaga, A. Züttel, L. Schlapbach, Acta Mater. 46 (1998) 4519.
[17] H. Takeshita, T. Oishi, N. Kuriyama, J. Alloys Compd. 333 (2002) 266.
[18] H. Kakuta, T. Miyashita, Y. Goto, A. Kamegawa, H. Takamura, M. Okada, Mater. Trans. 42 (2001) 443.
[19] K.E. Johansson, T. Palm, P.-E. Werner, J. Phys. E 13 (1980) 1289.
[20] P.-E. Werner, L. Eriksson, S. Salomé, SCANPI, A Program for Evaluating Guinier Photographs, Stockholm University, Stockholm, 1980.
[21] P.-E. Werner, L. Eriksson, M. Westdahl, J. Appl Crystallogr. 18 (1985) 367.

[22] P.-E. Werner, Ark. Kemi 31 (1969) 513.
[23] J. Rodriguez-Carvajal, FULLPROF Version 3.2 March 2005, ILL (unpublished).
[24] P.E. Blöchl, Phys. Rev. B 50 (1994) 17953;
G. Kresse, J. Joubert, Phys. Rev. B 59 (1999) 1758.
[25] G. Kresse, J. Hafner, Phys. Rev. B 47 (1993) 558;
G. Kresse, J. Furthmüller, Phys. Rev. B 54 (1996) 11169.
[26] J.P. Perdew, Y. Wang, Phys. Rev. B 45 (1992) 13244.
[27] H.J. Monkhorst, J.D. Pack, Phys. Rev. B 13 (1976) 5188.
[28] E. Rönnebro, D. Noréus, K. Kadir, A. Reiser, B. Bogdanovic, J. Alloys Compd. 299 (2000) 101.
[29] F. Gingl, T. Vogt, E. Akiba, K. Yvon, J. Alloys Compd. 282 (1999) 125.
[30] G. Renaudin, B. Bertheville, K. Yvon, J. Alloys Compd. 353 (2003) 175.
[31] In our calculations entropy and zero point energy contributions were not considered and it is therefore possible that compositions yielding slightly positive formation energies adopt the perovskite structure.
[32] E. Orgaz, M. Gupta, J. Alloys Compd. 209 (1994) 159;
E. Orgaz, M. Gupta, J. Alloys Compd. 231 (1995) 147.
[33] E. Orgaz, V. Mazel, M. Gupta, Phys. Rev. B 54 (1996) 16124.
[34] The so-called virtual-crystal approximation (VCA) is the simplest approximation in the hierarchy of mean-field approaches for the description of random disorder [J.S. Faulkner, Prog. Mater. Sci. 273 (1981) 3; F. Ducastelle, Order and Phase Stability in Alloys, North-Holland, Amsterdam, 1991]. The H position was treated as a fictitious atom with the nuclear charge 2/3 and a corresponding number of valence electrons as to force charge neutrality.
[35] T. Vegge, L.S. Hedegaard-Jensen, J. Bonde, T.R. Munter, J.K. Norskov, J. Alloys Compd. 386 (2005) 1.
[36] P. Zolliker, K. Yvon, P. Fischer, J. Schefer, Inorg. Chem. 24 (1985) 4177.
[37] M.O. Mårtensson, M. Kritikos, D. Noréus, J. Am. Chem. Soc. 121 (1999) 10908.
[38] M. Olofsson, M. Kritikos, D. Noréus, Inorg. Chem. 37 (1998) 2900.